The initial errors occurring over Pacific-Atlantic Oceans and exerting large disturbing effect on ENSO predictability

Guangshan Hou [a,b], Meiyi Hou [c,d,*], Wansuo Duan [a,b]

[a] LASG, Institute of Atmospheric Physics, Chinese Academy of Sciences, Beijing 100029, China
[b] University of Chinese Academy of Sciences, Beijing 100049, China
[c] Yunnan Key Laboratory of Meteorological Disasters and Climate Resources in the Greater Mekong Subregion, Yunnan University, Kunming 650091, China
[d] Department of Atmospheric Sciences, Yunnan University, Kunming 650091, China

ABSTRACT

Using a novel data analysis method for predictability dynamics, the impacts of initial sea surface temperature (SST) errors over Pacific and Atlantic Oceans on the predictability of eastern and central Pacific El Niño (i.e., EP and CP El Niño) are investigated. The results reveal the initial SST errors that cause large disturbing effects on EP and CP El Niño forecasting, respectively. These initial errors are both exhibiting a positive-negative-positive-negative-positive chain structure along the direction from northwest to southeast over the Pacific for EP and CP El Niño, which resemble a combined mode of North Pacific Victoria Mode (VM), eastern tropical Pacific positive SST pattern (ETPPSP), and South Pacific meridional mode (SPMM); simultaneously, they exhibit a positive-negative meridional dipole pattern over South Atlantic, referred to as South Atlantic subtropical dipole mode (SASD); additionally, there exist initial warm SST anomalies in the equatorial Atlantic for EP El Niño and in the north tropical Atlantic for the CP El Niño. The above initial errors lead to the underestimation of both CP and EP El Niño. Further analyses illustrate that the initial warm SST errors in the north tropical Atlantic are positively correlated with the VM-like error pattern, which competed with the effect of the ETPPSP, makes the intensity of CP El Niño underestimated; whereas the SASD-like error pattern is revealed to have a positive relationship with the SPMM-like error mode, which only exists during EP El Niño period and interacts with the ETPPSP for much weak EP El Niño intensity. It is obvious that, for predicting which type of El Niño will occur, attention should also be paid to the initial sea temperature accuracy in the Atlantic Ocean under the interference effect of the Pacific Ocean temperature uncertainties.

1. Introduction

El Niño-Southern Oscillation (ENSO) is the combination of El Niño events, with abnormally warming in the tropical central-eastern Pacific, and the southern oscillation, with a dipole pattern in sea level pressure on the east and west sides of the tropical Pacific (Bjerknes, 1969). ENSO is the dominant inter-annual climate variability in the tropical Pacific, affecting weather and climate on a global scale through atmospheric teleconnections and even exerting severe meteorological disasters (Andrews et al. 2004; Hansen et al.

1998; Joly and Voldoire, 2009; Lyon and Camargo, 2008; Villafuerte and Matsumoto, 2015; Zhang et al. 2016). Therefore, it is important to predict El Niño events accurately.

Intensive studies have been made to understand the dynamic and physical mechanisms of ENSO, helping improve the physical process in numerical models to better depict the feature of ENSO evolution (Battisti and Hirst, 1989; Fang and Mu, 2018; Jin 1997a, 1997b; Picaut et al. 1997; Wang et al. 1999; Weisberg and Wang, 1997). However, the skill of real-time prediction of ENSO has not been improved as expected at the beginning of the twenty-first century (Barnston et al. 2012). One important reason is the frequent occurrence of atypical El Niño events during the recent three decades (Barnston et al. 2012; Tang et al. 2018). Differentiated by the warming center of the sea surface temperature anomaly (SSTA), the new flavor of El Niño is denoted as central Pacific (CP) El Niño while the canonical El Niño is recognized as eastern Pacific (EP) El Niño. The two types of El Niño events differ in not only the location of the largest SSTAs but also several other aspects, namely intensities, evolutionary trajectories, physical mechanisms, global influences, etc. (Ashok et al. 2007; Karori et al. 2013; Kug et al. 2009; Timmermann et al. 2018; Wu et al. 2012; Xiang et al. 2013). The frequent occurrence of CP El Niño brings up the need to distinguish El Niño events in advance, thus posing new challenges to real-time El Niño predictions. Hendon et al. (2009) and Lim et al. (2009) made effective predictions of the different SSTA patterns between two types of El Niño events using the Australian Bureau of Meteorology coupled ocean-atmosphere seasonal forecast model only one season ahead. Jeong et al. (2012) extended the lead time of prediction to four months by utilizing the multi-model ensemble mean data. Ren et al. (2019) demonstrated that only a minority of models could distinguish EP and CP El Niño within the leading time of one month. Ham et al. (2019) also indicated that only the deep-learning-based model was able to predict the spatial complexity of El Niño events to some extent. By applying the nonlinear forcing singular vector-based tendency perturbation forecast method to an intermediate-complexity ENSO model, Tao et al. (2020) extended the lead time to two seasons to distinguish the main characteristics of EP and CP El Niño. Furthermore, Zheng et al. (2023) generalized this method to an ensemble version and further extended the lead time to eight months. However, they only applied their method to the Zebiak-Cane model, which does not include the extratropical and forcing effects from other basins. Therefore, it is still necessary to further investigate how to improve the prediction skill of two types of El Niño with more comprehensive consideration.

One effective way to improve El Niño prediction skills is to reduce the initial errors of the predictions (Chen and Cane, 2008; Chen et al. 2004; Jin et al. 1994). Since ENSO occurs in the Pacific Ocean, the initial ocean temperature accuracy in the Pacific is important for improving the prediction of two types of El Niño events. Previous studies indicated that the initial errors inducing huge ENSO prediction errors have certain spatial patterns (Hou et al. 2019; Qi et al. 2021; Tian and Duan, 2016). Using the Zebiak-Cane model, Tian and Duan (2016) traced the evolution of a conditional nonlinear optimal perturbation that acts as the ocean temperature initial errors most interfere with the El Niño predictions. They found that the initial errors that cause large prediction errors of both El Niño events are mainly concentrated in the equatorial central and eastern Pacific. Hou et al. (2019) investigated the influence of initial sea temperature accuracy in tropical and extratropical Pacific on El Niño predictions by using an approach to data analysis for prediction. They illustrated that the initial ocean temperature accuracy in the Victoria mode region north of the Pacific is more important for better prediction of the intensity of CP El Niño and the structure of EP El Niño. The subsurface layer of the equatorial western Pacific and the surface layer of the southeast Pacific are more efficient for better prediction of the intensity of EP El Niño and the structure of CP El Niño. Qi et al. (2021) further confirmed this through sensitivity experiments.

Recently, many studies suggested that anomalous signals from other basins can affect ENSO variability in various ways. The SST variations in the tropical Indian Ocean could influence the following year's El Niño through atmospheric teleconnection as well as the oceanic channel (Annamalai et al. 2010; Dommenget et al. 2006; Izumo et al. 2010; Kug and Kang, 2006; Luo et al. 2010; Yuan et al. 2013; Yuan et al. 2011). Zhou et al. (2019) indicated that the initial errors associated with the Indian Ocean Dipole mode frequently induce the spring predictability barrier for El Niño events, and the corresponding sensitive area over the tropical Indian Ocean also be identified by applying targeted observation experiments (Zhou et al. 2020) Besides, the gradually increasing influence of the Atlantic Ocean is exerted on the tropical Pacific through different physical mechanisms (Cai et al. 2019; Li et al. 2016; McGregor et al. 2014). Specifically, negative equatorial Atlantic SST variability can trigger an El Niño event in subsequent winter by modulating Walker circulation (Ding et al. 2012); the north tropical Atlantic SST variabilities modulate El Niño through a Gill-type Rossby-wave response (Ham et al. 2013b; Wang et al. 2017; Wu et al. 2005); the South Atlantic subtropical dipole mode has an impact on ENSO by also modulating the Walker circulation (Bombardi et al. 2014; Boschat et al. 2013; Ham et al. 2021). In addition, it has been suggested that different parts of the Atlantic affect different parts of the Pacific, thus modulating the formation of different ENSO types (Ding et al. 2019; Dommenget and Yu, 2017; Ham et al. 2013a). Ham et al. (2013a) discovered that the SST variability in the north tropical Atlantic tends to impact the central Pacific, while the SST anomalies in the equatorial Atlantic mainly exert influences on the eastern Pacific. Ding et al. (2019) demonstrated that the anomaly signals from the north tropical Atlantic could serve as a unique precursor for the CP El Niño. In any case, all these studies suggest the important role of the Atlantic factors in modulating the formation of different types of ENSO. Therefore, it is necessary to study the effect of the Atlantic uncertainties on different types of ENSO predictability.

To our knowledge, various works have been performed to explore the relationship between the SSTA patterns in the Atlantic and the ENSO events, while the research on the contribution of the Atlantic SSTA accuracy to ENSO predictions is lacking. Frauen and Dommenget (2012) investigated the influence of the tropical Atlantic Ocean on the predictability of ENSO by using a general circulation model (GCM) coupled with an ENSO recharge oscillator ocean model. They indicated that removing the initial SST anomalies in the tropical Atlantic leads to a reduced prediction skill for Niño3 SSTA. Keenlyside et al. (2013) further elaborated that the knowledge of equatorial Atlantic SST enhances the predictions of El Niño. Exarchou et al. (2021) also confirmed this by using an ensemble seasonal forecast system. However, the above research mainly focused on the predictability of EP El Niño and did not emphasize the role of specific SST error patterns.

As reviewed above, the Atlantic factors have the potential effect on the evolution and diversity of El Niño. Therefore, it is natural

and crucial to explore the effect of the initial accuracy in the Atlantic Ocean on the prediction of two types of El Niño events. The present paper aims to answer the following question: Firstly, what kind of initial error pattern in the Atlantic and Pacific oceans most affects the prediction of two types of El Niño? Secondly, how can the initial errors in the Atlantic gradually evolve and eventually influence the prediction of two types of El Niño events? Lastly, how do different parts of the Atlantic and Pacific oceans interact in terms of modulating EP and CP El Niño events? Additionally, Hou et al. (2019) proposed a skillful and compute-saving approach to data analysis for predictability by using Coupled Model Intercomparison Project (CMIP) data, which can be perfectly utilized to achieve our goal in the present study.

This paper is organized as follows. In Section 2, a description of the CMIP model output and method used in this study are provided. Section 3 provide the spatial structure of initial SST errors in the Pacific and Atlantic, which induce the huge prediction errors of two type of El Niño and their effects. The interactions between different error structures over the Pacific and Atlantic will be discussed in Section 4. Finally, the study is concluded in Section 5.

2. Data and method

In the present study, we expect to analyze the initial errors that cause maximal prediction errors of two types of ENSO. Referring to the approach to data analysis for predictability dynamics (Hou et al. 2019), we use output data from pre-industrial (pi-control) runs of the CMIP5 (Coupled Model Inter-comparison Project Phase 5) climate model integrations. The pi-control experiment has fixed atmospheric composition, fixed solar variability, and constant background volcanic aerosol value. The output data is obtained after the model integration has reached stability. Therefore, the integration only includes the effects of internal variability, and its segments from different periods are equivalent theoretically. The 500-year integration period is chosen in the present study. Besides, based on the previous result of the model evaluation, we chose the CCSM4 climate model, which owns superior simulation skills for two types of El Niño events as well as the interaction process between tropical Pacific and other basins (Freund et al. 2020; Ham and Kug, 2015; Hou et al. 2022; Kim and Yu, 2012; Kucharski et al. 2015; Liu et al. 2021; Planton et al. 2021). The 500 years of sea surface temperature (SST), precipitation flux, and zonal and meridional wind monthly components derived from CCSM4 output are used. In order to facilitate analysis and calculation, all variables are interpolated onto the same grids (i.e., $1.0° \times 1.0°$) before analysis.

Based on the characteristics of dynamic differential equations and the seasonal cycle characteristics of oceanic and atmospheric variability, Hou et al. (2019) proposed a novel data analysis method on predictability to analyze the initial errors, which can exert significant influences on ENSO predictions. Specifically, a state variable in the ocean-atmosphere system is denoted as $U(X, t) = [U_1(\mathbf{X}, t), U_2(\mathbf{X}, t), ..., U_n(\mathbf{X}, t)], (\mathbf{X}, t) \in \Omega \times [0, T]$, where t stands for time. The governing equation of U can be written as:

$$\begin{cases} \dfrac{dU}{dt} = F(U, t) + f \\ U|_{t=0} = U_0 \end{cases} , \ in \quad \Omega \times [0, T]. \tag{1}$$

Herein, F is a nonlinear operator, U_0 is the initial state and f is the external forcing. Since the pi-control experiment utilizes a fixed external forcing, f is a constant. Then, integrate the equation from t_1 to t_2, the expression of U_2 at $t = t_2$ is written as follows:

$$U_2 = U_1 + \int_{t_1}^{t_2} F(U, t)dt + f(t_2 - t_1). \tag{2}$$

Eq. (2) can also be rewritten as:

$$U_2 = U_1 + M(U_1, t_1, t_2 - t_1) + f(t_2 - t_1). \tag{3}$$

M is the integral form of the nonlinear operator F.

Then, we select two time periods $[t_1, t_1 + \Delta t]$ and $[t_2, t_2 + \Delta t]$. It should be aware that the method we applied here is based on the variability of a climatological cycle like a seasonal cycle or a diurnal cycle. To make these two periods physically and mathematically comparable, t_1 and t_2 hold the same position in different cycles. For example, t_1 and t_2 are both January in different years. Integrate U during these two periods, the final states can be written as:

$$U_{t_2+\Delta t} = U_{t_2} + M(U_{t_2}, t_2, \Delta t) + f\Delta t. \tag{4}$$

$$U_{t_1+\Delta t} = U_{t_1} + M(U_{t_1}, t_1, \Delta t) + f\Delta t. \tag{5}$$

We subtract Eq. (5) from (4), the difference between $U_{t_2+\Delta t}$ and $U_{t_1+\Delta t}$ can be described as follows:

$$U_{t_2+\Delta t} - U_{t_1+\Delta t} = U_{t_2} - U_{t_1} + M(U_{t_2}, t_2, \Delta t) - M(U_{t_1}, t_1, \Delta t). \tag{6}$$

Based on the linear superposition of the solution of the equations and that t_1 and t_2 hold the same position in different cycles, Eq. (6) can also be rewritten as:

$$U_{t_2+\Delta t} - U_{t_1+\Delta t} = U_{t_2} - U_{t_1} + M(U_{t_2} - U_{t_1}, t_1(or \quad t_2), \Delta t). \tag{7}$$

As can be seen from the above equation, the difference between the final states $U_{t_2+\Delta t}$ and $U_{t_1+\Delta t}$ is only related to the difference of initial states U_{t_2} and U_{t_1} with the fixed integral interval length and the same position in the cyclic period of U. In addition, Eq. (7) and Eq. (4) share the same structure. That is $U_{t_2+\Delta t} - U_{t_1+\Delta t}$ also conforms to the development law of Eq. (4). The difference between
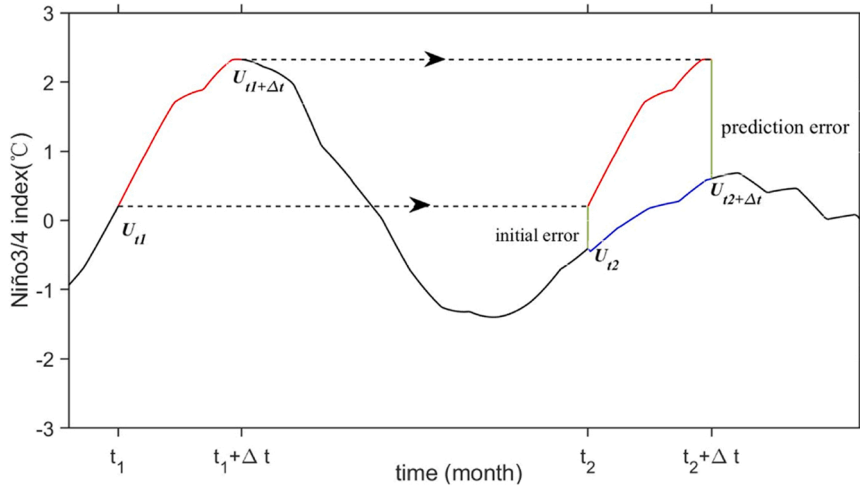
Fig. 1. Schematic diagram of the error growth.

$U_{t_2+\Delta t}$ and $U_{t_1+\Delta t}$ can be thought of derived by Eq. (4) with initial state $U_{t_2} - U_{t_1}$. As show in Fig. 1, different states during $[t_1, t_1 +\Delta t]$ and $[t_2, t_2 +\Delta t]$ are depicted as the red and blue curves. If we regard the states during these two segments as an "observation" and a "prediction" for the "observation", the initial difference, $U_{t_2} - U_{t_1}$, and the final difference, $U_{t_2+\Delta t} - U_{t_1+\Delta t}$, indicate the initial error and the prediction error, respectively. Therefore, Fig. 1 describes the development of the initial error which conforms to Eq. (4).

As discussed above, this method can be utilized to explore the development mechanism of the initial error without interference from model error. Since ENSO events are the primary source of interannual climate variability and have a strong seasonal cycle component. This approach can be applied to investigate the initial value problems for the ENSO predictability dynamics. Besides, in the study by Hou et al. (2019), this method was used to investigate the initial error in the Pacific Ocean that affects the two types of El Niño predictions the most. Their results were in agreement with the subsequent findings of Qi et al. (2021), who obtained initial errors over the Pacific for two types of El Niño predictions through sensitivity experiments. This verified the rationality of the method. In this study, we therefore use this method to investigate the initial error in both the Pacific and Atlantic oceans that have the significant influence on the prediction of two types of El Niño.

13 typical EP El Niño and 13 CP El Niño events are selected from the 500-year integration of the CCSM4 model and regarded as "observations", based on the criterion that Niño3 index for EP El Niño (Niño4 index for CP El Niño) is greater than 0.5 ℃ for 6 consecutive months and peaking in boreal winter. All the "observations" we selected in model stimulation contain states in the developing phase of the El Niño event from January to December, and peaking at the end of the year. For each selected one-year "observation", we pick the corresponding 20 one-year integration snippets before and after it. Then, 40 one-year integration segments are denoted as 40 "predictions" of the corresponding "observation", which was initiated in January with a lead time of 12 months. Thus, 520 predictions for each type of El Niño case are created. The prediction error can be described as follows:

$$\mathrm{E}(t) = \sqrt{\frac{1}{N}\sum_{(i,j)}\left[T^p_{(i,j)}(t) - T^o_{(i,j)}(t)\right]^2}.$$

Where $T^p_{(i,j)}$ represents the prediction value, $T^o_{(i,j)}$ represents the observation value, t denotes different prediction times from January to December, (i,j) is the grid points of the select region (Niño3 of EP El Niño, Niño4 for CP El Niño), and N is the total grid number of the selected region. All prediction errors conform to the evolution law of Eq. (7), only depending on the initial errors.

3. The initial errors inducing large prediction errors of two types of El Niño and their related error growth

3.1. The initial errors of two types of El Niño events

Our goal in this study is to investigate the initial SST errors in the Pacific and the Atlantic that most affect the predictions of two types of El Niño events. Therefore, we select the predictions only with huge prediction errors in December (i.e., prediction errors greater than average, 221 samples for CP El Niño and 253 for EP El Niño) from all of the 520 predictions. Then, an Empirical Orthogonal Function (EOF) analysis is applied to their initial errors with a spatial domain of the Pacific and Atlantic (66.5°S–66.5°N, 120°E–20°E). For CP El Niño, the first EOF mode explained 26.91% of the total variance, while for EP El Niño, the explained variance of the first EOF mode accounts for 38.84% of the total variance. The explained variances of the following EOF modes are small compared to the first one, inferring that the initial errors with structures resembling the first EOF mode, often have great impacts on the prediction of CP El Niño (EP El Niño). To pick out these initial error members with prominent influences, we utilize the principal component (PC) value as a measure of the spatial similarity between a single member and a specific EOF mode. The member with a PC
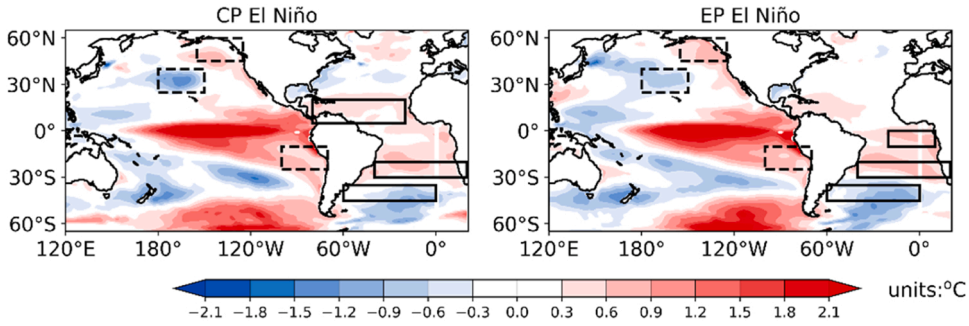
Fig. 2. Composites of initial SST error structures CP-type-error (left) and EP-type-error (right).

value greater (smaller) than the average of all positive (negative) PC values is regarded as highly positively (negatively) correlated with this EOF mode. According to this standard, four groups are selected from all prediction members, namely EP-EOF1 + , EP-EOF1-, CP-EOF1 + and CP-EOF1−. We calculate the Niño3 SSTA prediction errors at a 12-month lead time for all members in groups EP-EOF1- and EP-EPF1 + . It was revealed that the prediction errors generated by group EP-EOF1- are larger than those generated by group EP-EOF1 + . The same approach was also applied to CP El Niño. The Niño4 SSTA prediction errors at a 12-month lead time are calculated for members in groups CP-EOF1 +and CP-EOF1−. The result shows that the prediction errors generated by group CP-EOF1 + are greater than those by group CP-EOF1−. Therefore, we refer to the composite of the group EP-EOF1- and group CP-EOF1 + (illustrated in Fig. 2) as the main initial error structures that tend to cause significant prediction errors for EP El Niño and CP El Niño, and refer to these two kinds of errors as CP-type error and EP-type error hereafter.

As illustrated in Fig. 2, both CP-type and EP-type errors show great similarities in the Pacific region, presenting a meridional distribution of positive-negative-positive-negative-positive SST anomalies. A significant positive SST error center is located in the central-eastern tropical Pacific, denoted as the eastern tropical Pacific positive SST pattern (ETPPSP) hereafter. In the North Pacific, the SST errors are mainly located in two regions: positive anomalies in the Gulf of Alaska and negative anomalies in the southern Aleutian Islands. The positive-negative SST pattern along the direction from northeast to southwest shows a great resemblance to the Victoria Mode (VM) (Ding et al. 2015b). While in the South Pacific, the initial errors hold a positive-negative-positive meridional structure, with a northwest-southeast error chain in Easter Island, negative errors in the south-central Pacific, and positive errors in the northern side of the Bellingshausen Sea in Antarctica, which is similar to the South Pacific meridional mode (SPMM) (Min et al. 2017).

In terms of the Atlantic region, the structure of CP-type-error and EP-type-error in the South Atlantic are both exhibiting a meridional dipole pattern, resembling the South Atlantic subtropical dipole (SASD) mode (Venegas et al. 1997), with a positive error in the subtropical South Atlantic and a large negative error in the north of South Georgia Island. However, the error structures possess different distributions in the tropical Atlantic region for EP- and CP-type errors. For CP El Niño, the initial SST errors exhibit a broad range of positive SST anomalies in the north tropical Atlantic, while the positive errors in EP-type errors are more confined to the eastern area of the Caribbean Sea with weaker strength. Additionally, EP-type errors possess large positive errors over the eastern equatorial Atlantic.

3.2. The initial error evolutions of two types of El Niño events

To investigate how the CP-type and the EP-type errors over the Pacific and Atlantic evolve to affect the predictions of CP and EP El Niño, the evolutions of these initial errors are traced (Fig. 3). Since the El Niño prediction is the focus of our study, we concern about the error evolvement near Niño3 and Niño4 area. The developments for both error types over the tropical Pacific are similar to the transition from an El Niño event to a La Niña event. That is, the positive errors in topical Pacific gradually decay and eventually develop into an opposite pattern, inducing a cold bias of prediction in tropical central-eastern Pacific at a 12-month lead time. It is consistent with the conclusion demonstrated by Hou et al. (2019) that the initial errors inducing large prediction errors for El Niño develop similarly to a La Niña evolving mode. Zhang et al. (2015) also demonstrated that the optimal precursory disturbances of La Niña over the tropical Pacific resemble the optimal initial errors related to the spring predictability barrier for El Niño events, which means the initial errors could share a similar structure and evolving process with signals of corresponding opposite events. Moreover, as shown in Fig. 3e, j, the maximal prediction errors in the tropical Pacific for CP El Niño are more westly and weaker than those for EP El Niño. It is also in line with actual observations that CP El Niño has a weaker phase transition process than EP El Niño (Kug et al. 2009).

As outlined in Section 2, it has been proved mathematically that the errors are governed by the same dynamic equations as the corresponding state variables in the dynamic model, which means that the evolution of initial errors shares the same physical mechanisms as the corresponding state variables in the dynamic model. Therefore, the error evolution can be interpreted by the physical mechanism that explains how the actual state variables evolve. For the Pacific Ocean, from a physical perspective, the positive SST errors in the central-eastern tropical Pacific with westerly wind anomalies over the central Pacific (Fig. 3a.f), generate upwelling Rossby waves off the equator propagating westward through the Ekman transport. Simultaneously, in the extratropical Pacific, the VM-like SST error pattern and the SPMM-like error are all concomitant with local low-level cyclonic errors. For the VM-like error
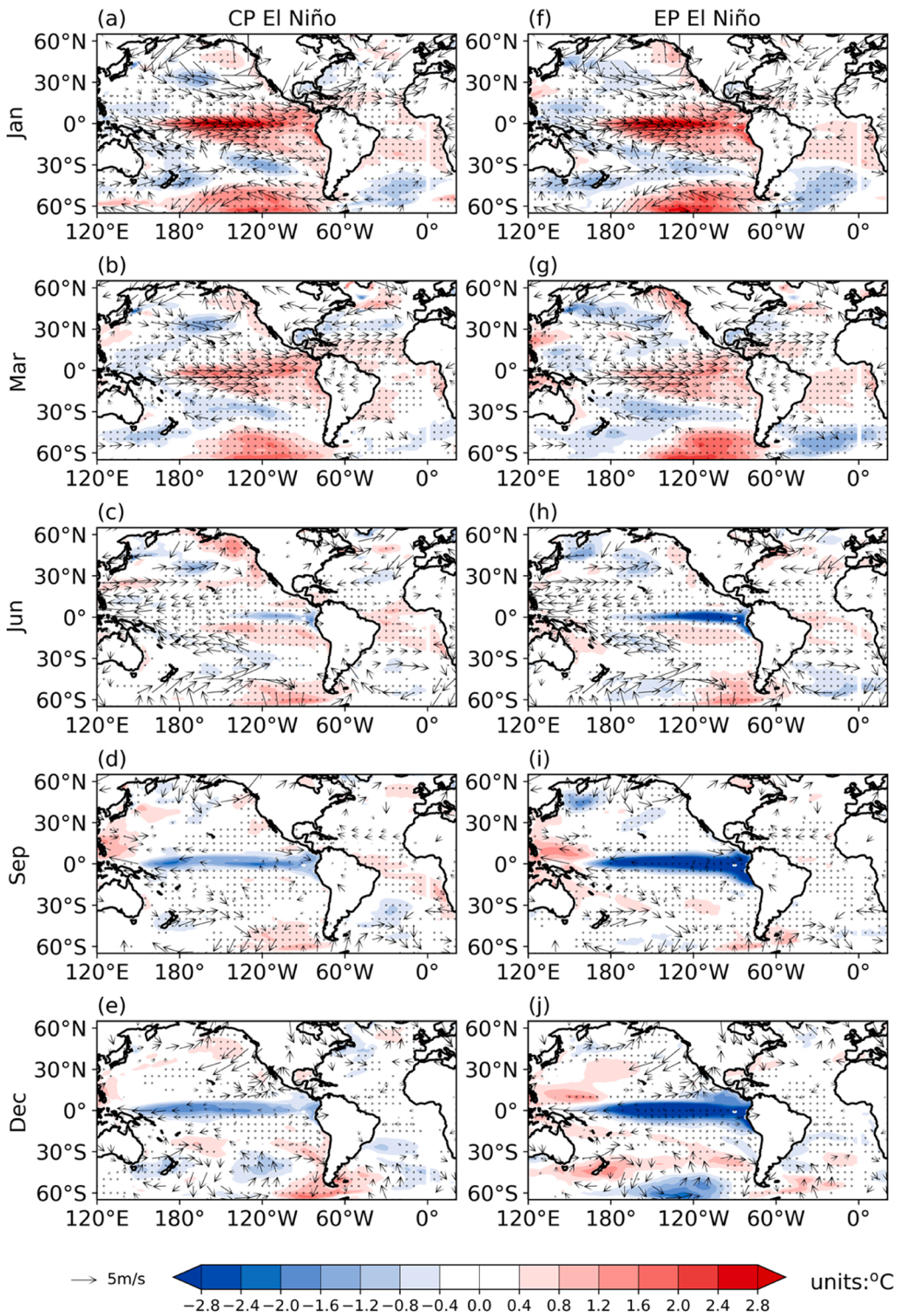
Fig. 3. (a)-(e) Composite of SST errors (units: ℃) and 850hPa wind errors (units: m/s) of CP El Niño in January, March, June, September, and December. (f)-(j) same as (a)-(e), but for EP El Niño. The dote areas denote these exceed 0.05 significance level.

pattern, consistent with these cyclonic anomalies, the westerly anomalies occur in its south, inducing the positive surface temperature errors to propagate southwestward via the WES mechanism. Meanwhile, over the South Pacific, the wind anomalies also play a role in promoting the maintenance of the local positive errors and their further propagation to the eastern equatorial Pacific. Over time, the
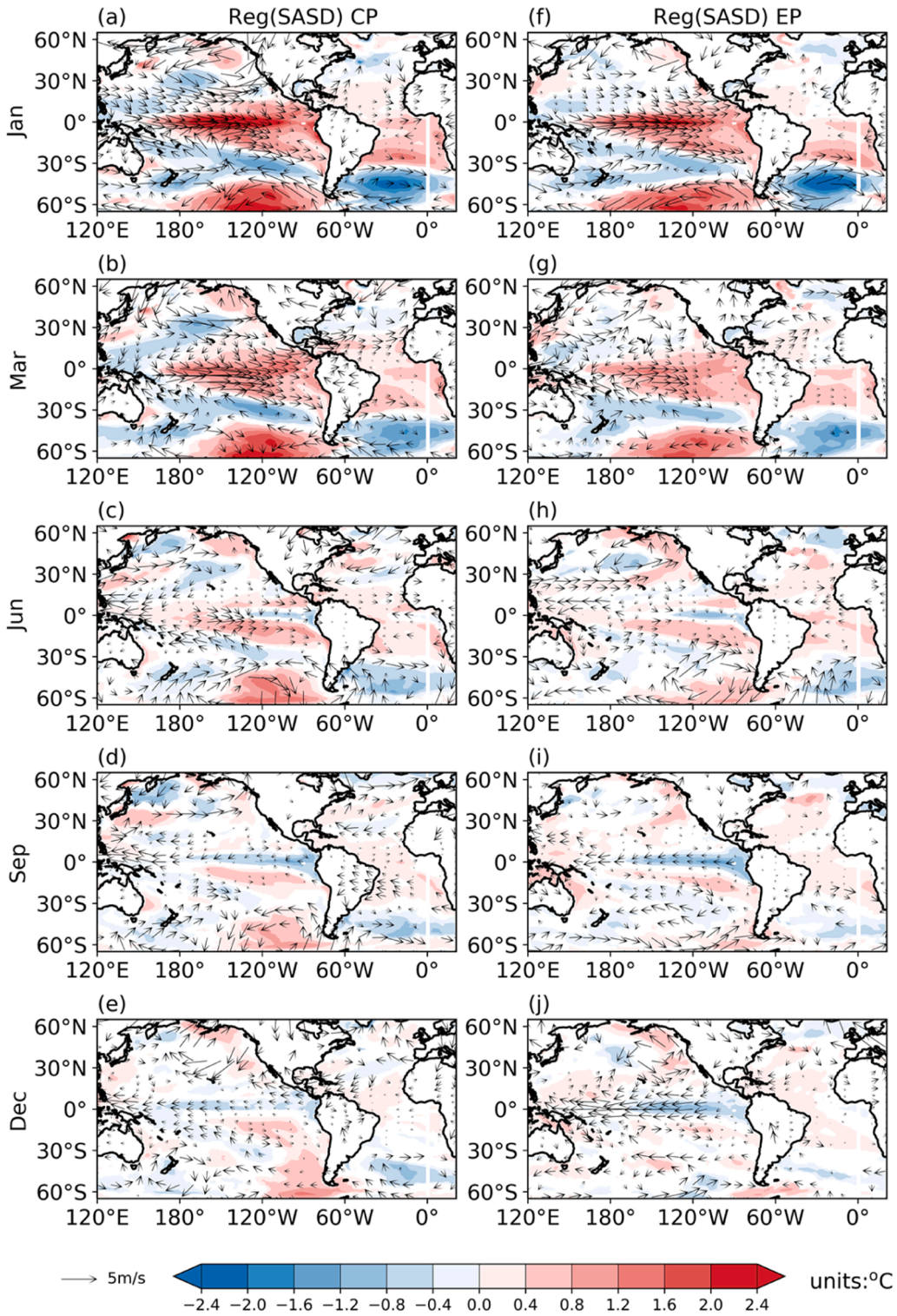
Fig. 4. (a)-(e) lagged regressions of averaged SST initial error over South Atlantic ((40°W-20°E, 30°S-20°S) subtracted (60°W-0°, 45°S-35°S)) with SST errors and 850hPa wind errors for CP El Niño. (f)-(j) same as (a)-(e), but for EP El Niño. Only those exceeding the 0.05 significance level are shown.
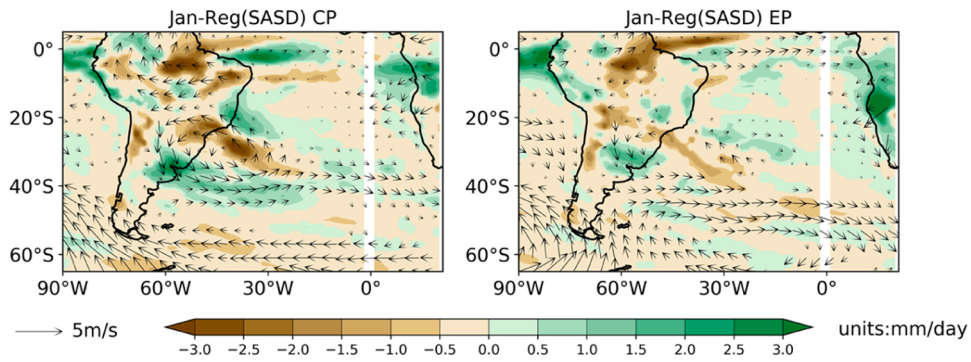
Fig. 5. regressions of averaged SST initial error over South Atlantic ((40°W-20°E, 30°S-20°S) subtracted (60°W-0°, 45°S-35°S)) with precipitation errors and 850hPa wind error.

upwelling Rossby wave generated by ETPPSP errors continues to propagate westward. Once they reach the western boundary of the Pacific, part of the wave is reflected to form upwelling equatorial Kelvin waves that propagate eastward. The reflected Kelvin waves induce shoaling of the thermocline and transport subsurface negative errors in the equatorial western Pacific upward and eastward, playing a cooling role over the eastern Pacific (Fig. 3c, h). After the negative SST errors appear over the equatorial eastern Pacific, easterly wind anomalies will be generated (Fig. 3c, h). The process will be then amplified through Bjerknes feedback (Bjerknes, 1969). The precipitation changes over the western Pacific can also amplify it by modulating ocean stratification and then feeding back to SST errors (Zhang and Busalacchi, 2009). Eventually, significant negative errors gather around the equatorial central-eastern Pacific, leading to underestimating the intensity of CP and EP El Niño. However, over the North Pacific region, due to the strong initial SST errors in the tropical Pacific and their opposite role in the prediction errors at the end of the year, the southwestward propagation of initial errors over the North Pacific is weakened, which can only delay or suppress the development of cold SST errors in the equatorial region rather than determine. Similar to the situation in the South Pacific, the corresponding wind and SST errors have become weaker and decay rapidly, nearly disappearing (Fig. 3e, h) after June.

Compared with the initial errors in the Pacific, those in the Atlantic are weaker in intensity. In addition, the initial errors in the Atlantic influence ENSO prediction by their transportation to the Pacific region. The evolving process of the initial errors in the Atlantic is hard to recognize in Fig. 3. Therefore, an extraction of the error-evolving process for the initial errors in the Atlantic is necessary. As previously illustrated, SASD-like initial error structure in the South Atlantic, positive errors in the equatorial Atlantic, and north tropical Atlantic are three main parts of the initial errors in the Atlantic. To better investigate the effects of the initial SST errors in these different parts of the Atlantic, we construct the SST initial error indexes based on these three areas that are illustrated in Fig. 2 and then obtain error variables using lagged regressions on the corresponding error fields.

The SASD-like initial error index is derived by subtracting the average of SST initial error over 60°W-0°, 45°S-35°S from the average of SST initial error over 40°W-20°E, 30°S-20°S (shown in Fig. 2 solid black line boxes, refers to the definition by Ham et al. (2021)). As previously illustrated, the SASD-like initial error structure is inclined to exert great influences on both types of El Niño. Therefore, we obtain the error-evolving process related to the SASD-like initial errors by regressing the SASD-like error index on both EP and CP El Niño error fields. The lag regression results are shown in Figs. 4 and 5. From a physical perspective, the meridional SST dipole structure in the South Atlantic boosts a concomitant low-level anomalous cyclonic circulation in southeastern South America (Fig. 4a, f). The low-level convergence anomalies further reinforce the frequency of low-level jets, affecting moisture transport from Amazon to southeastern South America (Bombardi et al. 2014), resulting in decreasing precipitation over the South Atlantic Convergence Zone (SACZ) (Fig. 5). Subsequently, the anomalous latent heat release generates Kelvin waves to propagate eastward, leading to the anomalous westerly wind errors over the equatorial Atlantic (Ham et al., 2021), then inducing positive SST errors in the equatorial Atlantic through Bjerknes feedback mechanism (Fig. 4b, g). Eventually, the warm SST errors modulate Walker circulation, thereby promoting the decaying of the positive errors in the equatorial Pacific (Fig. 4.c-e, h-j). Compared with the regression of EP and CP El Niño, the final SST errors caused by SASD-like error pattern are slightly greater in the situation of EP El Niño, whereas the errors are further west with a larger range and a smaller magnitude in the case of CP El Niño. Thus, when the error pattern is superimposed on EP El Niño, it mainly affects El Niño's intensity, while superimposed on the CP El Niño, not only is the intensity of CP El Niño under-estimated but also its structure affected.

Similarly, we construct the NTA initial error index from the area average of SST initial error over 80°W-20°W, 5°N-20°N and EA initial error index from the area average of SST initial error over 20°W-10°E, 10°S-0° based on the large area on the previous EOF analyses (shown in Fig. 2 solid black line boxes). Different from the SASD-like error structure, the positive errors in the north tropical Atlantic are more likely to have a greater impact on the prediction of CP El Niño, while the errors in the equatorial Atlantic prefer to impact EP El Niño events. Therefore, the regression analyses related to the NTA initial errors are only applied to the CP El Niño error fields in subsequent analyses. For the initial error in the EA, its regression analyses only applied to EP El Niño error fields.

The error-evolving process related to the NTA error index by regressing on CP El Niño error fields is shown in Fig. 6a-e. Positive error in the north tropical Atlantic boosts low-level cyclonic wind anomalies in the north tropical Atlantic and southern North America (Fig. 6a). The northeasterly wind anomalies associated with the anomalous cyclone offset by the southwesterly wind anomalies related
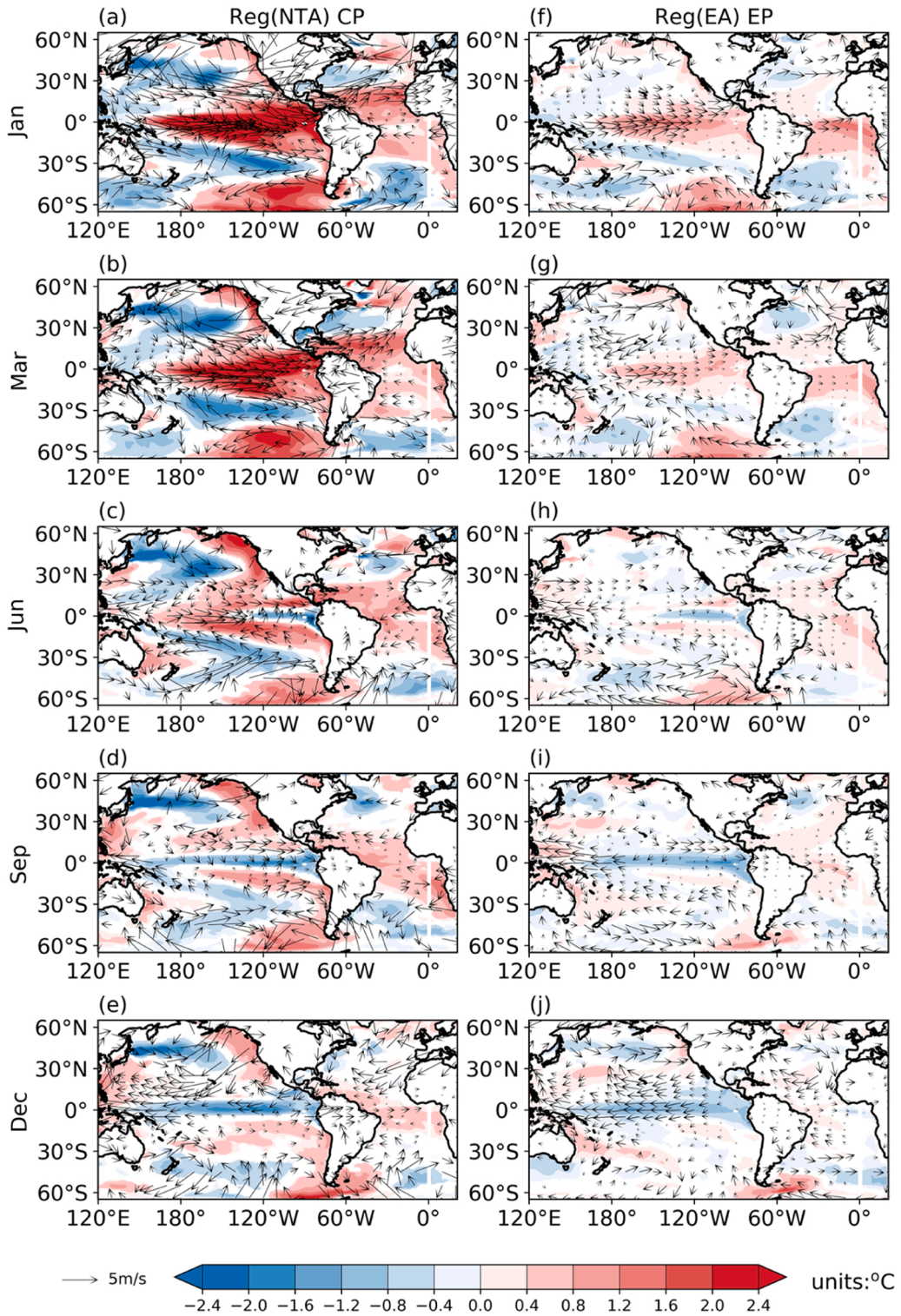
Fig. 6. (a)-(e) lagged regressions of averaged SST initial error in north tropical Atlantic (80°W-20°W, 5°N-20°N) with SST errors and 850hPa wind errors for CP El Niño. (f)-(j) same as (a)-(e), but over equatorial Atlantic (20°W-10°E, 10°S-0°) for EP El Niño. Only those exceeding the 0.05 significance level are shown.
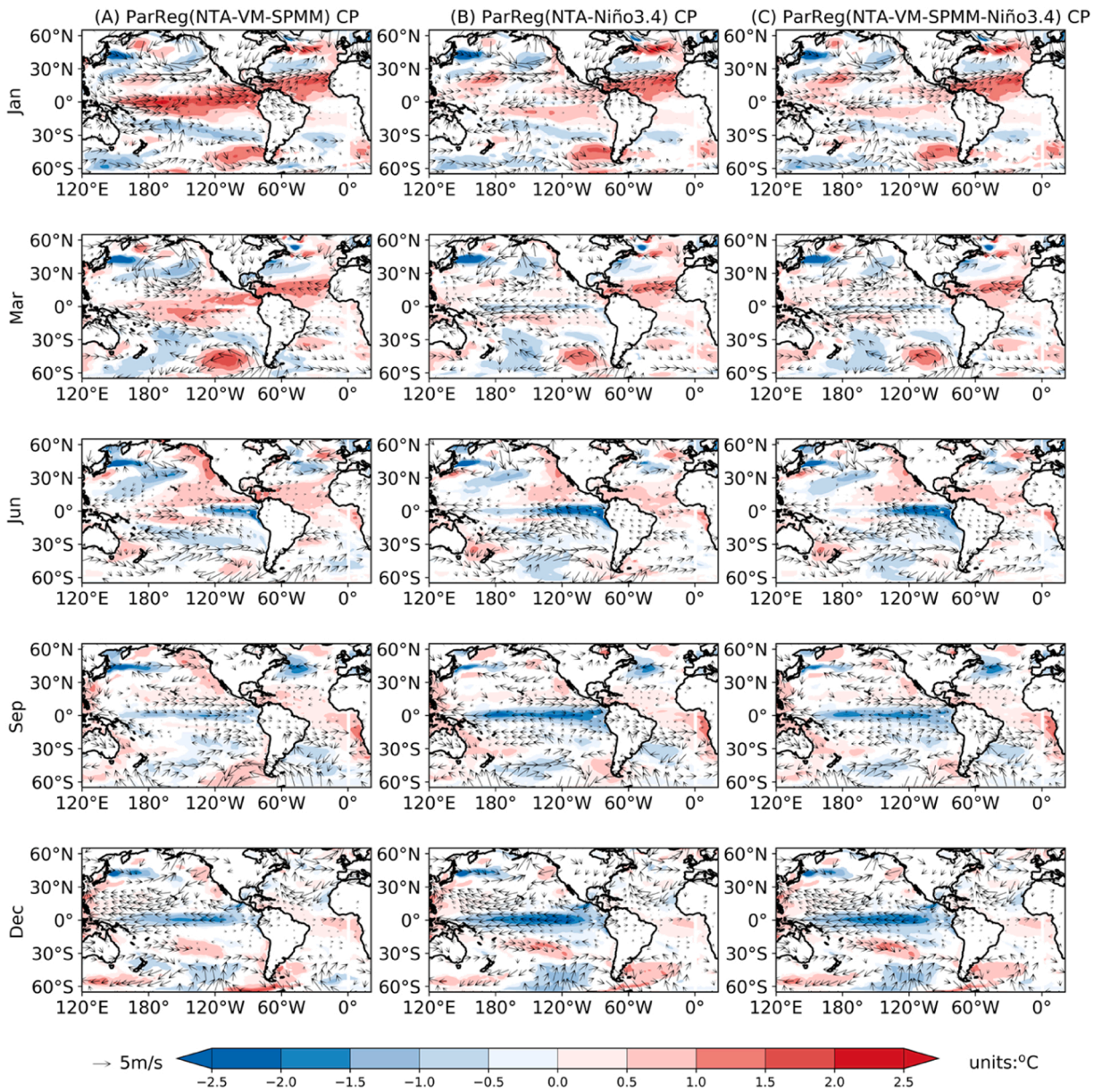
Fig. 7. lagged regressions of (A) averaged SST initial error over north tropical Atlantic onto SST errors and 850hPa wind errors excluding the impact of VM-like initial error ((155°−125°W, 45°N-60°N) subtracted (180°−150°W, 25°N-40°N), dash black line boxes in Fig. 2) and SPMM-like initial error (100°W-70°W, 25°S-15°S, dash black line boxes in Fig. 2) for CP El Niño; (B) same area but excluding the impact of initial error over Niño3.4 (170°W-120°W, 5°S-5°N); (C) same area but excluding the impact of VM-like and SPMM-like error pattern and the initial errors in tropical Pacific (Niño3.4); Only those exceed the 0.05 significance level are shown.

to the cyclone generated by the VM-like SST error in the northeastern subtropical Pacific (Fig. 6a-c). It weakens the positive contribution of the VM-like initial error pattern proposed to the SST errors in the northern subtropical Pacific region, and indirectly promotes the decline of the positive errors and the formation of negative errors in the equatorial central-eastern Pacific, causing the under-prediction of CP El Niño events. As for the initial errors in the equatorial Atlantic, from a physical perspective, the positive errors in the equatorial Atlantic modify local horizontal wind convection (Fig. 6f), causing the abnormally ascending motion over the eastern equatorial Atlantic. Then, the abnormal vertical motion further induced the modulation of Walker circulation, resulting in the abnormal sinking in the tropical eastern Pacific. The descending and motion anomalies in the tropical eastern Pacific generated a low-level divergence anomaly (Fig. 6h, i), thus suppressing local convection and westerly wind anomalies, facilitating the cold bias growth over the equatorial Pacific. Thereby, the positive errors in the equatorial Atlantic would underestimate the intensity of EP El Niño and even make the prediction result tend to be predicted as an EP La Niña event.
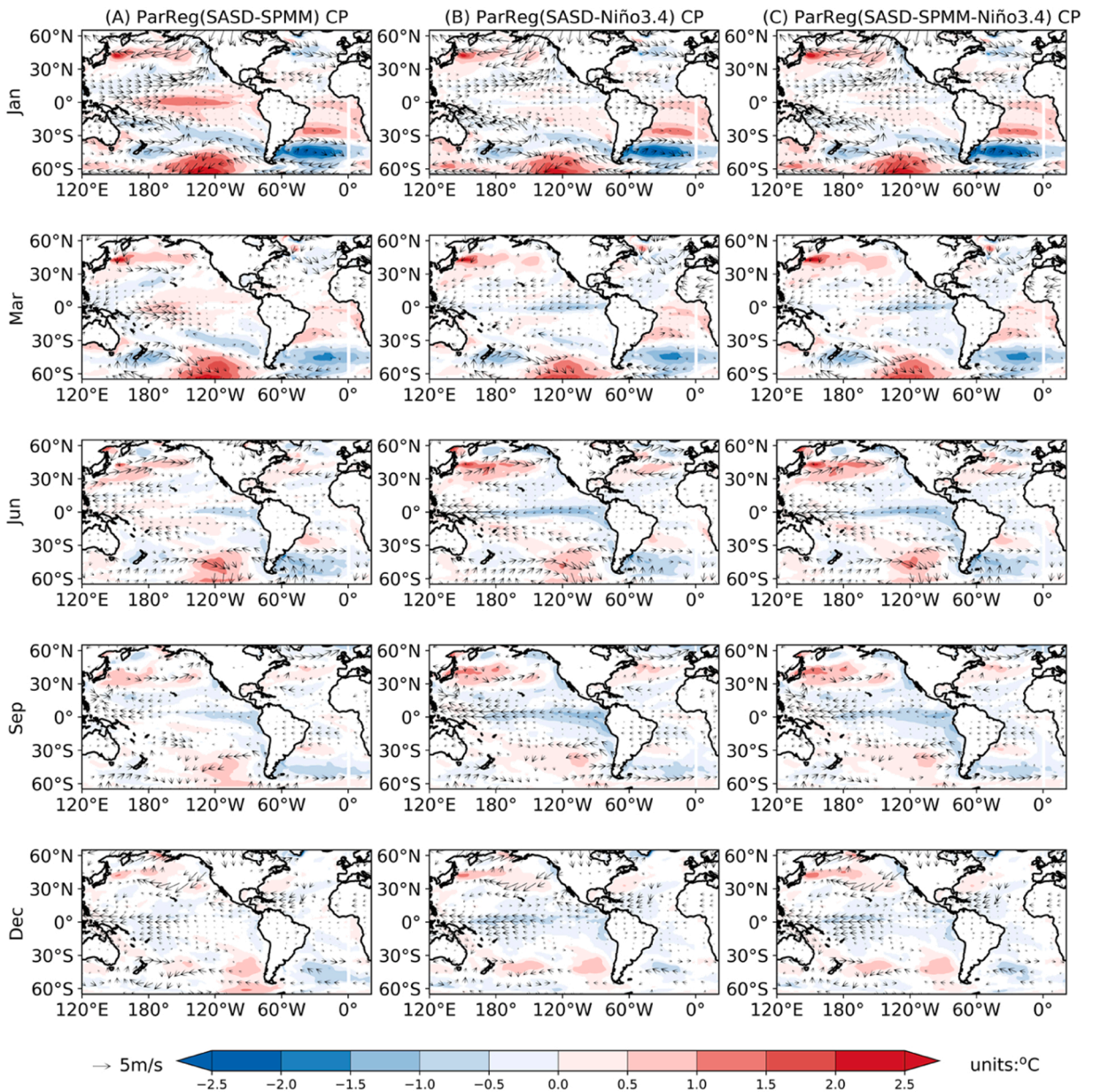
Fig. 8. lagged regressions of (A) averaged SST initial error South Atlantic subtropical dipole onto SST errors and 850hPa wind errors excluding the impact of VM-like initial error and SPMM-like initial error for CP El Niño; (B) same area but excluding the impact of initial error over Niño3.4; (C) same area but excluding the impact of VM-like and SPMM-like error pattern and the initial errors in tropical Pacific (Niño3.4); Only those exceed the 0.05 significance level are shown.

In summary, the evolution of the SST errors over the tropical Pacific evolves like a decay mode of El Niño and then a developing mode of La Nina. During the whole process, the ETPNSP error pattern promotes the formation of negative errors, while the initial error patterns in the extratropical Pacific play an opposite role. In the Atlantic, all three major error structures of both types of errors facilitate the growth of cold errors in the tropical Pacific, leading to a colder bias in El Niño prediction, but their specific effects on the two types of El Niño prediction differ. The SASD-like error pattern is manifested in both EP- and CP-type errors. For EP El Niño, the prediction errors caused by it are larger and more confined to the tropical eastern Pacific, underestimating the intensity of EP El Niño. By contrast, there are weaker cold SST prediction errors over the whole tropical Pacific in the situation of CP El Niño, influencing the structure and intensity of CP El Niño predictions. At the same time, both the positive initial SST errors in the north tropical Atlantic of CP-type error and in the equatorial Atlantic of EP-type error are inclined to underestimate the corresponding El Niño events. However, due to the strong initial SST errors in the tropical Pacific, those over the extra-tropical Pacific and Atlantic tend to modulate the El Niño predictions rather than determine during the whole process. The presence of cold prediction errors in the tropical Niño-related areas in
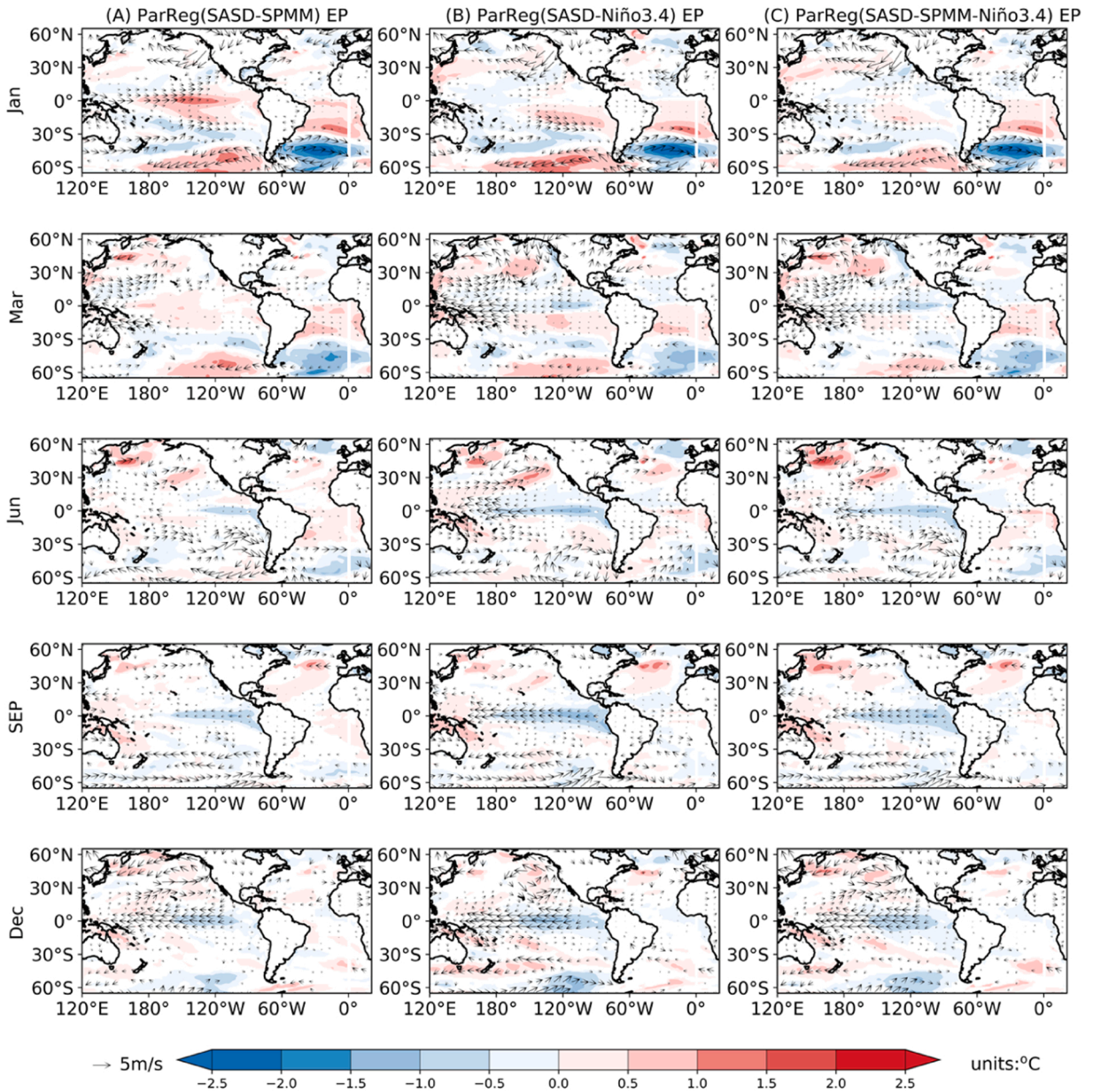
Fig. 9. Same as Fig. 8 but for EP El Niño.

December indicates that the evolutionary process of the initial errors in the equatorial Pacific and in the Atlantic outperforms that in the extratropical Pacific.

4. Interactions of errors over Pacific and Atlantic

In the previous section, we obtain the initial SST error structures, which exert great impacts on the predictions of two types of El Niño events in the Pacific and Atlantic. The evolutions and specific influences on different types of El Niño events of these initial error patterns are also investigated. It is worth noting that the SST initial errors in different areas can exert different effects on the formation of the final negative error in the equatorial Pacific. In addition, the VM-like error mode and SPMM-like error mode also exist when regressing the NTA error for CP El Niño in January (Fig. 6a), implying the possibility of the connection of error structures in different ocean basins in predicting CP El Niño events.

To clarify the physical mechanism of this connection, three partial regression experiments are designed. Firstly, the effects of VM-like and SPMM-like error patterns are removed using linear regression before the lagged regressions are calculated with an error index constructed in the large initial SST error region of NTA like the approach using in Section 3.2 to get rid of the original influence of the

VM-like and SPMM-like errors. As shown in Fig. 7A, the SPMM-like error pattern and its associated cyclonic anomalies become inconspicuous. However, low-level cyclonic wind anomalies over the North Pacific still exist. The wind anomalies associated with the cyclone reduce the sea surface evaporation near the Gulf of Alaska and enhance the evaporation over the central North Pacific, further inducing a VM-like error pattern in the North Pacific. Consistent with the cyclonic anomalies, the southwesterly wind anomalies over the subtropical North Pacific promote the formation and further southwestward propagation of positive errors via the WES mechanism. This process suppresses or delays the cold error formation in the tropical central Pacific. However, the positive errors in the north tropical Atlantic boost an anomalous cyclone in the region. The northeasterly wind anomalies associated with the anomalous cyclone then facilitate the formation of negative SST errors in the north subtropical Pacific, propagating the abnormal signal through the Gill-type Rossby-wave response (Ham et al. 2013b). This eventually accelerates the development of negative error over the tropical central Pacific. These two processes fight against each other in the subtropical North Pacific, ultimately altogether influencing the SST errors in the tropical central Pacific.

In addition, the anomalous cyclone in the North Pacific can also be affected by the SST errors in the equatorial central-eastern Pacific through teleconnection. The interference is therefore eliminated by calculating lagged regressions after removing the linear regression with respect to Niño3.4 SST errors. According to the regression results (Fig. 7B), the intensity of the VM-like and SPMM-like error patterns are significantly weakened, which corroborates that the positive SST errors in the equatorial Pacific have a positive effect on these two error modes. And because of the elimination of positive SST errors in the tropical Pacific in January, the transition from positive to negative errors is faster and earlier, leading to a stronger negative error structure in December. What calls for special attention is that even though the intensity of the VM-like and SPMM-like error patterns are significantly weakened, the weakened anomalous cyclone in the North Pacific still exists. It further indicates that the positive SST errors in the north tropical Atlantic are linked to the VM-like SST error pattern in the North Pacific through certain atmospheric teleconnection mechanism. Furthermore, an analogous result was also obtained by removing the effects of both VM-like and SPMM-like error patterns and Niño3.4 SST errors (Fig. 7C). The anomalous cyclone also exists in the regression result of January, further proving our inference.

Similar to the regression results of positive initial errors in NTA for CP El Niño, the connection of error structures in different ocean basins also exists in the lagged regression results of the SASD-like error pattern for CP El Niño. The SPMM-like error pattern appears in the regression results of the SASD-like error index in January, interfering with the influence of the SASD-like error on the CP El Niño predictions. Therefore, to further analyze whether a coadjutant effect exists between these two types of error modes and eliminate the interference of SST errors on equatorial Pacific, we also conducted three partial regression analyses: (1) remove the effect of SPMM-like error pattern; (2) remove the influence of the initial errors in tropical Pacific (Niño3.4); (3) remove the effects of SPMM-like error pattern and the initial errors in tropical Pacific. The results are illustrated in Fig. 8. After eliminating the effect of the anomalous SST signal in the tropical Pacific (Fig. 8B), the intensity of the SPMM-like error pattern becomes extremely weak. It seems to imply that the SPMM-like error pattern in the regression result of SASD-like errors for CP El Niño might be a mirage-like phenomenon caused by SST signals in the tropical Pacific. Compared with the intensity of the negative SST errors in the tropical Pacific in December, three different regression conditions lead to similar results. The only difference between analysis 1 and analysis 2 in December is caused by the positive SST errors in the tropical Pacific in January. From this perspective, it demonstrates that the SPMM-like error structure in the regression results of the SASD-like error pattern for CP El Niño is caused by the interference of SST errors in the tropical Pacific.

In the situation of EP El Niño, the regression result of the SASD-like error pattern shows remarkable resemblances to that for CP El Niño containing the SPMM-like error mode in January. Thus, the same partial regression analyses are conducted for EP El Niño as those for CP El Niño. Unlike the regression results for CP El Niño, after eliminating the effect of the SST errors in the tropical Pacific (Fig. 9B), the intensity of the SPMM-like error pattern becomes slightly weak, but the mode still exists. And there are also cyclonic anomalies accompanying the SPMM-like error pattern. Due to its weak strength, the error pattern rapidly collapses in March, illustrating that a positive connection between the SASD-like error pattern and SPMM-like error pattern exists in the situation of EP El Niño predictions. However, the SPMM-like error pattern suppresses the formation of negative errors in the equatorial Pacific via the WES mechanism. While the meridional diploe error structure in the South Atlantic plays a positive role in the formation of positive SST errors in the equatorial Atlantic by influencing diabatic heating and further modulating Walker circulation, thereby promoting a cold bias in the equatorial Pacific. The two error patterns compete with each other and interact with ETPPSP, causing an underestimation of EP El Niño. Compared with the partial regression results for CP El Niño, the connection between SASD-like error pattern and SPMM-like error pattern only seems to exist in the situation of EP El Niño. For CP El Niño, the appearance of the SPMM-like error pattern in the regression results of the SASD-like error pattern is just interference of SST errors in the tropical Pacific.

Through the above regression experiments, those initial SST error patterns in the tropical Atlantic and South Atlantic connect with initial error modes in the extratropical Pacific. The results reveal that there is a positive correlation between the positive SST errors in the north tropical Atlantic and the VM-like SST error pattern. However, due to their opposite role in affecting the low-level wind anomalies in the subtropical North Pacific, their effect on the error evolving process in the tropical central Pacific are competitive, thus leading to an inconspicuous result compared with the result without removing the effects of VM-like and SPMM-like error patterns. In the situation of EP El Niño predictions, the SASD-like error pattern is revealed to exert a positive connection to the SPMM-like error pattern, whereas it is almost nonexistent in the case of CP El Niño. It seems to imply that the connection between the SASD-like error pattern and the SPMM-like error pattern might be affected by different physical mechanisms in the case of two different types of El Niño. Moreover, these two error patterns also have opposite effects on El Niño predictions. In conclusion, the initial error in the different parts of the Atlantic Ocean can affect El Niño predictions by interfering with the initial error in the Pacific Ocean. The initial SST accuracies in the Atlantic also play an essential role in both types of El Niño predictions, considering the influences and the interactions of different error patterns.

5. Summary and discussion

In the present study, we investigated the initial error over the Pacific and Atlantic exerting large disturbing effects on different types of El Niño from the perspective of initial error growth. By analyzing structures of initial SST errors over the Pacific and Atlantic via a novel data analysis method for the predictability dynamics of climate events, we obtain two error types that cause great influences on the predictions of CP and EP El Niño events, respectively. Both types of errors exhibit a positive-negative-positive-negative-positive-negative meridional chain structure in the whole Pacific. Specifically, they possess a positive-negative-positive triple-like shape over the North Pacific and South Pacific, referred to as positive Victoria Mode and positive South Pacific Meridional Mode. As for the equatorial Pacific, a wide range of positive SST errors (ETPPSP) are shown in the equatorial central-eastern Pacific for both error types. Simultaneously, the initial SST errors over the Atlantic are weaker but also show large-scale spatial structures, implying the importance of initial errors with specific structures for the two types of El Niño predictions. In the South Atlantic, they present a positive-negative meridional diploe pattern for both types of El Niño, resembling the South Atlantic subtropical meridional mode. Additionally, it is worth noting that the initial errors possess different structures in the tropical Atlantic. There are a range of warm SST errors in the north tropical Atlantic for CP El Niño; while for EP El Niño, they exhibit a warm SST pattern in the equatorial eastern Atlantic.

By tracing the evolution of errors, we show that, for both CP El Niño and EP El Niño, the SST errors over the tropical Pacific behave like El Niño decay and transform into an opposite phase developing. It should be noted that the prediction errors are a result of the combined influence of initial errors in different regions. Therefore, we further investigate the error-evolving processes of different initial error patterns to clarify the effects of different error patterns. Either for CP El Niño or EP El Niño, the positive initial SST errors in the eastern equatorial Pacific (ETPPSP) promote the formation of negative errors, causing the underestimation of the intensity of El Niño. While in the extratropical Pacific, both VM-like and SPMM-like initial error patterns tend to suppress or delay the development of negative errors in the tropical Pacific. But the effect of the VM-like error pattern is more westerly, whereas the influence of the SPMM-like error pattern is more confined to the equatorial eastern Pacific early in the decline of El Niño. As a result, the VM-like initial errors are more likely to affect the intensity of CP El Niño and the structure of EP El Niño; the SPMM-like errors tend to influence the intensity of EP El Niño and the structure of CP El Niño. For the Atlantic, the positive-negative meridional dipole mode in the South Atlantic subtropical region is influential in predicting the intensity of EP El Niño and the structure of CP El Niño. The initial errors in the north tropical Atlantic and in the equatorial Atlantic are prone to underestimate the intensity of CP El Niño and EP El Niño, respectively. For the positive SST errors at $60°$S over the South Pacific are similar to a quadrupole SSTA pattern identified by Ding et al. (2015a). They suggested that the anomaly signal in the mid-latitude South Pacific could impart an SST footprint to extend through the subtropical southeastern Pacific to the tropical Pacific via the WES mechanism. However, our study found that the subtropical errors over the South Pacific decrease rapidly. The corresponding low-level wind anomalies in the evolution of CP-type and EP-type errors also decay faster, which could be attributed to low-level wind errors in the subtropical southeastern region and the model bias over the mid-latitude and subtropical South Pacific. Therefore, it seems that the influence of the errors in the mid-latitude South Pacific is not as evident as other errors in the Pacific in the present study.

Furthermore, to figure out how different error patterns connect each other and make a joint effect on the formation of SST errors in the tropical Pacific, we conducted several partial regression experiments. The positive initial errors in the north tropical Atlantic are revealed to be linked to the VM-like SST error pattern in the North Pacific through some atmospheric teleconnection mechanisms. Due to their opposite role in influencing low-level wind anomalies in the northern subtropical Pacific, they fight against one another, ultimately affecting error evolution in the tropical central Pacific. We also discovered that the SASD-like error pattern in the southern Atlantic shows a positive connection with the SPMM-like error mode. What calls for special attention is that the connection seems to be evident only in the situation of EP El Niño events, and almost nonexistent in the case of CP El Niño events. Interestingly, these two error patterns also have opposite effects on El Niño. Nonetheless, we have only verified the positive connections between the error patterns on the Atlantic and extratropical Pacific through regression experiments. Further investigation needs to be undertaken regarding the interaction between these error patterns and to what extent they can contribute to El Niño predictions.

It has to be acknowledged that, due to the strong positive initial errors in the tropical Pacific, the initial errors over the tropical Pacific play a more dominant role in predicting two types of El Niño, those over the extratropical Pacific and Atlantic tend to modulate the El Niño predictions. Since the tropical Pacific is the base map of ENSO, it is reasonable that the tropical Pacific is crucial for the prediction of ENSO than other ocean basins. Nonetheless, our results indicate that there do exist large-scale initial error spatial structures in the tropical Atlantic and South Atlantic regions, which often lead to large prediction errors. And it has been proved that these SST anomaly structures can evolve and modulate the SST errors in the tropical Pacific through certain physical mechanisms. Therefore, even though the initial SST errors over the Atlantic are weaker than those of the tropical Pacific, Atlantic influence on SST predictions of the tropical Pacific is essential. Furthermore, since both types of error possess large-scale spatial structures over the Atlantic, it provides a clue to identify the sensitive area in the Atlantic for the predictions of both types of El Niño. If additional observations are adopted in these areas, the prediction error may be reduced when simulating in the model.

Tian and Duan (2016) investigate the influence of tropical Pacific uncertainties on CP and EP El Niño predictions. They emphasized the importance of initial sea temperature error over tropical central-eastern Pacific in distinguishing the type of El Niño events. Hou et al. (2019) further considered the extratropical Pacific influence on El Niño uncertainties besides the tropical, especially for those associated with the predictability barrier, by applying the same data analysis method as the present study. Their results revealed the difference between the North and South Pacific initial sea temperature uncertainties on the effects of different types of El Niño predictions. In the present study, homogeneous initial error patterns over the tropical and extratropical Pacific are also obtained. We also emphasized the dominant role of the accuracy of the sea temperature in the tropical Pacific and the effects of the extratropical Pacific on modulating El Niño predictions. Besides, we additionally focused on the Atlantic sea surface temperature accuracy on different
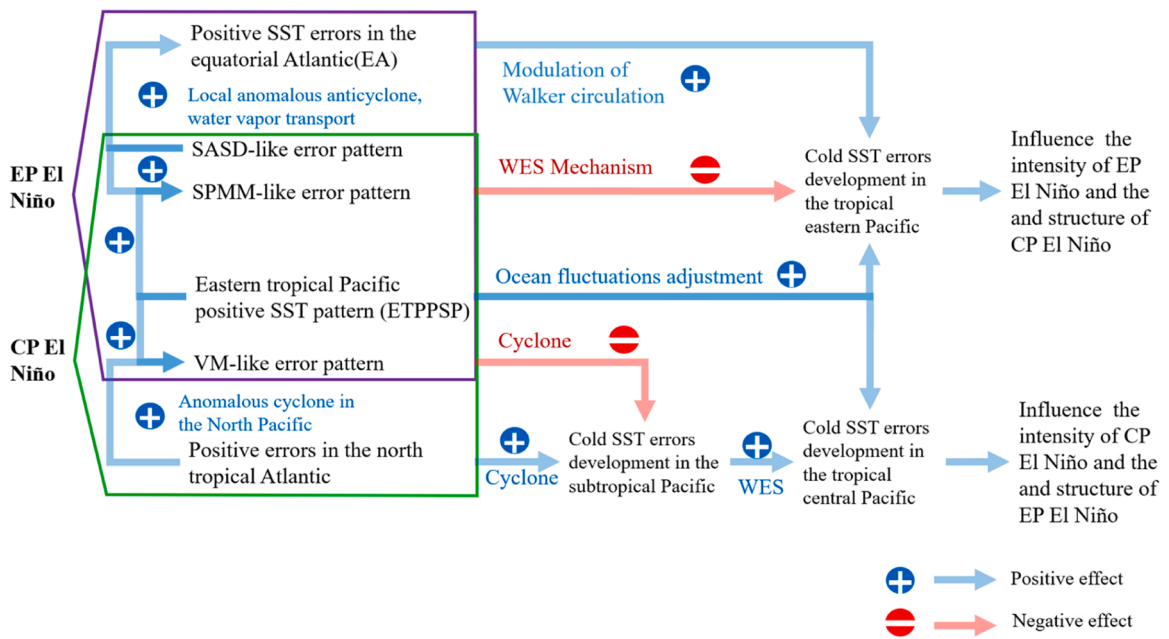
Fig. 10. Schematic diagram of impacts of initial SST errors in the Pacific and Atlantic Oceans on the prediction of two types of El Niño.

types of El Niño prediction uncertainties. We discovered that the positive initial errors in the north tropical Atlantic are prone to be more influential on CP El Niño events, while the positive initial errors in the equatorial Atlantic tend to underestimate the EP El Niño prediction. It further suggested that different types of El Niño events have different mechanisms for their development. A schematic digraph containing all the initial error modes over the Pacific and Atlantic and their dynamics influencing the two types of El Niño predictions is shown in Fig. 10.

A novel data analysis method for predictability is applied in the present study, which can be easily calculated by using only model long-term integration results. However, because of no running sensitivity model experiments, it isn't easy to explicitly quantify influences that different areas of the Atlantic and Pacific contribute to two types of El Niño predictions. Further investigations are still urged to be undertaken in the future. Nevertheless, our result demonstrated the synergistic effect of the Atlantic with the extratropical Pacific on the predictions of two types of El Niño events and emphasized the importance of the initial accuracy of sea surface temperature over the Atlantic in two types of El Niño predictions, implying the possible sensitive area over the Atlantic Ocean for targeted observations. Besides, the growing sum of research focuses on interactions between the Atlantic, Pacific and Indian Ocean (Wang, 2019). Several studies also show that initial accuracy over the Indian Ocean contributes to ENSO predictions (Zhou et al. 2019; Zhou et al. 2020). Further investigations could be launched to explore the Indian Ocean effect on three-ocean interactions and its interaction with the Pacific and Atlantic Oceans in contributing to the predictability of different types of El Niño events.

CRediT authorship contribution statement

Guangshan Hou: Conceptualization, Formal analysis, Investigation, Software, Visualization, Writing – original draft. **Meiyi Hou:** Conceptualization, Funding acquisition, Methodology, Supervision, Writing – review & editing. **Wansuo Duan:** Conceptualization, Funding acquisition, Project administration, Writing – review & editing.

Declaration of Competing Interest

The authors declare that they have no known competing financial interests or personal relationships that could have appeared to influence the work reported in this paper.

Data Availability

Data will be made available on request.

Acknowledgements

References

Andrews, E.D., Antweiler, R.C., Neiman, P.J., Ralph, F.M., 2004. Influence of ENSO on flood frequency along the California Coast. J. Clim. 17, 337–348.

Annamalai, H., Kida, S., Hafner, J., 2010. Potential impact of the tropical indian ocean–indonesian seas on El Niño characteristics. J. Clim. 23, 3933–3952.

Ashok, K., Behera, S.K., Rao, S.A., Weng, H., Yamagata, T., 2007. El Niño Modoki and its possible teleconnection. J. Geophys. Res. 112.

Barnston, A.G., Tippett, M.K., L'Heureux, M.L., Li, S., Dewitt, D.G., 2012. Skill of real-time seasonal ENSO model predictions during 2002–11: is our capability increasing? Bull. Am. Meteorol. Soc. 93, 631–651.

Battisti, D.S., Hirst, A.C., 1989. Interannual variability in a tropical atmosphere–ocean model: influence of the Basic State, Ocean Geometry and Nonlinearity. J. Atmos. Sci. 46, 1687–1712.

Bjerknes, J., 1969. atmospheric teleconnections from the equatorial Pacific. Mon. Weather Rev. 97, 163–172.

Bombardi, R.J., Carvalho, L.M.V., Jones, C., Reboita, M.S., 2014. Precipitation over eastern South America and the South Atlantic Sea surface temperature during neutral ENSO periods. Clim. Dyn. 42, 1553–1568.

Boschat, G., Terray, P., Masson, S., 2013. Extratropical forcing of ENSO. Geophys. Res. Lett. 40, 1605–1611.

Cai, W., et al., 2019. Pantropical climate interactions. Science **363**.

Chen, D., Cane, M.A., 2008. El Niño prediction and predictability. J. Comput. Phys. 227, 3625–3640.

Chen, D., Cane, M.A., Kaplan, A., Zebiak, S.E., Huang, D., 2004. Predictability of El Niño over the past 148 years. Nature 428, 733–736.

Ding, H., Keenlyside, N.S., Latif, M., 2012. Impact of the equatorial atlantic on the El Niño Southern oscillation. Clim. Dyn. 38, 1965–1972.

Ding, R., Li, J., Tseng, Y.-H., 2015a. The impact of South Pacific extratropical forcing on ENSO and comparisons with the North Pacific. Clim. Dyn. 44, 2017–2034.

Ding, R., Li, J., Tseng, Y.-H., Sun, C., Guo, Y., 2015b. The Victoria mode in the North Pacific linking extratropical sea level pressure variations to ENSO. J. Geophys. Res.: Atmospheres 120, 27–45.

Ding, R., Li, J., Tseng, Y.H., Sun, C., Li, Y., Xing, N., Li, X., 2019. Linking the North American Dipole to the Pacific Meridional Mode. J. Geophys. Res.: Atmospheres 124, 3020–3034.

Dommenget, D., Yu, Y., 2017. The effects of remote SST forcings on ENSO dynamics, variability and diversity. Clim. Dyn. 49, 2605–2624.

Dommenget, D., Semenov, V., Latif, M., 2006. Impacts of the tropical Indian and Atlantic Oceans on ENSO. Geophys. Res. Lett. 33.

Exarchou, E., Ortega, P., Rodriguez-Fonseca, B., Losada, T., Polo, I., Prodhomme, C., 2021. Impact of equatorial Atlantic variability on ENSO predictive skill. Nat. Commun. 12, 1612.

Fang, X.-H., Mu, M., 2018. A three-region conceptual model for central pacific El Niño including zonal advective feedback. J. Clim. 31, 4965–4979.

Frauen, C., Dommenget, D., 2012. Influences of the tropical Indian and Atlantic Oceans on the predictability of ENSO. Geophys. Res. Lett. 39 (n/a-n/a).

Freund, M.B., Brown, J.R., Henley, B.J., Karoly, D.J., Brown, J.N., 2020. Warming patterns affect El Niño diversity in CMIP5 and CMIP6 models. J. Clim. 33, 8237–8260.

Ham, Y.-G., Kug, J.-S., 2015. Role of north tropical atlantic SST on the ENSO simulated using CMIP3 and CMIP5 models. Clim. Dyn. 45, 3103–3117.

Ham, Y.-G., Kug, J.-S., Park, J.-Y., 2013a. Two distinct roles of Atlantic SSTs in ENSO variability: North Tropical Atlantic SST and Atlantic Niño. Geophys. Res. Lett. 40, 4012–4017.

Ham, Y.-G., Kim, J.-H., Luo, J.-J., 2019. Deep learning for multi-year ENSO forecasts. Nature 573, 568–572.

Ham, Y.-G., Kug, J.-S., Park, J.-Y., Jin, F.-F., 2013b. Sea surface temperature in the north tropical Atlantic as a trigger for El Niño/Southern Oscillation events. Nat. Geosci. 6, 112–116.

Ham, Y.G., Lee, H.J., Jo, H.S., Lee, S.G., Cai, W., Rodrigues, R.R., 2021. Inter-Basin Interaction Between Variability in the South Atlantic Ocean and the El Niño/Southern Oscillation. Geophys. Res. Lett. 48.

Hansen, J.W., Hodges, A.W., Jones, J.W., 1998. ENSO Influences on Agriculture in the Southeastern United States. J. Clim. 11, 404–411.

Hendon, H.H., Lim, E., Wang, G., Alves, O., Hudson, D., 2009. Prospects for predicting two flavors of El Niño. Geophys. Res. Lett. 36.

Hou, M., Duan, W., Zhi, X., 2019. Season-dependent predictability barrier for two types of El Niño revealed by an approach to data analysis for predictability. Clim. Dyn. 53, 5561–5581.

Hou, M., Tang, Y., Duan, W., Shen, Z., 2022. Toward an optimal observational array for improving two flavors of El Niño predictions in the whole Pacific. Clim. Dyn. 60, 831–850.

Izumo, T., et al., 2010. Influence of the state of the Indian Ocean Dipole on the following year's El Niño. Nat. Geosci. 3, 168–172.

Jeong, H.-I., et al., 2012. Assessment of the APCC coupled MME suite in predicting the distinctive climate impacts of two flavors of ENSO during boreal winter. Clim. Dyn. 39, 475–493.

Jin, F.-F., 1997a. An Equatorial Ocean Recharge Paradigm for ENSO. Part II: A Stripped-Down Coupled Model. J. Atmos. Sci. 54, 830–847.

Jin, F.-F., 1997b. An Equatorial Ocean Recharge Paradigm for ENSO. Part I: Conceptual Model. J. Atmos. Sci. 54, 811–829.

Jin, F.F., Neelin, J.D., Ghil, M., 1994. El Nino on the Devil's Staircase: Annual Subharmonic Steps to Chaos. Science 264, 70–72.

Joly, M., Voldoire, A., 2009. Influence of ENSO on the West African Monsoon: Temporal Aspects and Atmospheric Processes. J. Clim. 22, 3193–3210.

Karori, M.A., Li, J., Jin, F.-F., 2013. The Asymmetric Influence of the Two Types of El Niño and La Niña on Summer Rainfall over Southeast China. J. Clim. 26, 4567–4582.

Keenlyside, N.S., Ding, H., Latif, M., 2013. Potential of equatorial Atlantic variability to enhance El Niño prediction. Geophys. Res. Lett. 40, 2278–2283.

Kim, S.T., Yu, J.-Y., 2012. The two types of ENSO in CMIP5 models. Geophys. Res. Lett. 39 (n/a-n/a).

Kucharski, F., Syed, F.S., Burhan, A., Farah, I., Gohar, A., 2015. Tropical Atlantic influence on Pacific variability and mean state in the twentieth century in observations and CMIP5. Clim. Dyn. 44, 881–896.

Kug, J.-S., Kang, I.-S., 2006. Interactive Feedback between ENSO and the Indian Ocean. J. Clim. 19, 1784–1801.

Kug, J.-S., Jin, F.-F., An, S.-I., 2009. Two Types of El Niño Events: Cold Tongue El Niño and Warm Pool El Niño. J. Clim. 22, 1499–1515.

Li, X., Xie, S.-P., Gille, S.T., Yoo, C., 2016. Atlantic-induced pan-tropical climate change over the past three decades. Nat. Clim. Change 6, 275–279.

Lim, E.-P., Hendon, H.H., Hudson, D., Wang, G., Alves, O., 2009. Dynamical forecast of Inter–El Niño variations of tropical SST and Australian spring rainfall. Mon. Weather Rev. 137, 3796–3810.

Liu, M., Ren, H.-L., Zhang, R., Ineson, S., Wang, R., 2021. ENSO phase-locking behavior in climate models: from CMIP5 to CMIP6. Environ. Res. Commun. 3.

Luo, J.-J., Zhang, R., Behera, S.K., Masumoto, Y., Jin, F.-F., Lukas, R., Yamagata, T., 2010. Interaction between El Niño and Extreme Indian Ocean Dipole. J. Clim. 23, 726–742.

Lyon, B., Camargo, S.J., 2008. The seasonally-varying influence of ENSO on rainfall and tropical cyclone activity in the Philippines. Clim. Dyn. 32, 125–141.

McGregor, S., Timmermann, A., Stuecker, M.F., England, M.H., Merrifield, M., Jin, F.-F., Chikamoto, Y., 2014. Recent Walker circulation strengthening and Pacific cooling amplified by Atlantic warming. Nat. Clim. Change 4, 888–892.

Min, Q., Su, J., Zhang, R., 2017. Impact of the South and North Pacific Meridional Modes on the El Niño–Southern Oscillation: Observational Analysis and Comparison. J. Clim. 30, 1705–1720.

Picaut, J., Masia, F., du Penhoat, Y., 1997. An Advective-Reflective Conceptual Model for the Oscillatory Nature of the ENSO. Science 277, 663–666.

Planton, Y.Y., et al., 2021. Evaluating Climate Models with the CLIVAR 2020 ENSO Metrics Package. Bull. Am. Meteorol. Soc. 102, E193–E217.

Qi, Q., Duan, W., Xu, H., 2021. The most sensitive initial error modes modulating intensities of CP- and EP- El Niño events. Dyn. Atmospheres Oceans 96.

Ren, H.-L., et al., 2019. Seasonal predictability of winter ENSO types in operational dynamical model predictions. Clim. Dyn. 52, 3869–3890.

Tang, Y., et al., 2018. Progress in ENSO prediction and predictability study. Natl. Sci. Rev. 5, 826–839.

Tao, L., Duan, W., Vannitsem, S., 2020. Improving forecasts of El Niño diversity: a nonlinear forcing singular vector approach. Clim. Dyn. 55, 739–754.

Tian, B., Duan, W., 2016. Comparison of the initial errors most likely to cause a spring predictability barrier for two types of El Niño events. Clim. Dyn. 47, 779–792.

Timmermann, A., et al., 2018. El Nino-Southern Oscillation complexity. Nature 559, 535–545.

Venegas, S.A., Mysak, L.A., Straub, D.N., 1997. Atmosphere–Ocean Coupled Variability in the South Atlantic. J. Clim. 10, 2904–2920.

Villafuerte, M.Q., Matsumoto, J., 2015. Significant Influences of Global Mean Temperature and ENSO on Extreme Rainfall in Southeast Asia. J. Clim. 28, 1905–1919.

Wang, C., 2019. Three-ocean interactions and climate variability: a review and perspective. Clim. Dyn. 53, 5119–5136.

Wang, C., Weisberg, R.H., Virmani, J.I., 1999. Western Pacific interannual variability associated with the El Niño-Southern Oscillation. J. Geophys. Res.: Oceans 104, 5131–5149.

Wang, L., Yu, J.Y., Paek, H., 2017. Enhanced biennial variability in the Pacific due to Atlantic capacitor effect. Nat. Commun. 8, 14887.

Weisberg, R.H., Wang, C., 1997. A western pacific oscillator paradigm for the El Niño-Southern oscillation. Geophys. Res. Lett. 24, 779–782.

Wu, L., He, F., Liu, Z., 2005. Coupled ocean-atmosphere response to north tropical Atlantic SST: Tropical Atlantic dipole and ENSO. Geophys. Res. Lett. 32.

Wu, R., Chen, J., Chen, W., 2012. Different Types of ENSO Influences on the Indian Summer Monsoon Variability. J. Clim. 25, 903–920.

Xiang, B., Wang, B., Li, T., 2013. A new paradigm for the predominance of standing Central Pacific Warming after the late 1990s. Clim. Dyn. 41, 327–340.

Yuan, D., Zhou, H., Zhao, X., 2013. Interannual climate variability over the tropical pacific ocean induced by the Indian Ocean dipole through the Indonesian throughflow. J. Clim. 26, 2845–2861.

Yuan, D., et al., 2011. Forcing of the Indian Ocean dipole on the interannual variations of the tropical pacific ocean: roles of the indonesian throughflow. J. Clim. 24, 3593–3608.

Zhang, J., Duan, W., Zhi, X., 2015. Using CMIP5 model outputs to investigate the initial errors that cause the "spring predictability barrier" for El Niño events. Sci. China Earth Sci. 58, 685–696.

Zhang, R.-H., Busalacchi, A.J., 2009. Freshwater Flux (FWF)-Induced Oceanic Feedback in a Hybrid Coupled Model of the Tropical Pacific. J. Clim. 22, 853–879.

Zhang, W., et al., 2016. Unraveling El Niño's impact on the East Asian Monsoon and Yangtze River summer flooding. Geophys. Res. Lett. 43.

Zheng, Y., Duan, W., Tao, L., Ma, J., 2023. Using an ensemble nonlinear forcing singular vector data assimilation approach to address the ENSO forecast uncertainties caused by the "spring predictability barrier" and El Niño diversity. Clim. Dyn.

Zhou, Q., Mu, M., Duan, W., 2019. The initial condition errors occurring in the indian ocean temperature that cause "spring predictability barrier" for El Niño in the Pacific Ocean. J. Geophys. Res.: Oceans 124, 1244–1261.

Zhou, Q., Duan, W., Hu, J., 2020. Exploring sensitive area in the tropical Indian Ocean for El Niño prediction: implication for targeted observation. J. Oceanol. Limnol. 38, 1602–1615.